

# A Visual Perception-Based Tunable Framework and Evaluation Benchmark for H.265/HEVC ROI Encryption

Xiang Zhang, Geng Wu, Wenbin Huang, Daoyong Fu, Fei Peng, Zhangjie Fu

**Abstract**—ROI selective encryption, as an efficient privacy protection technique, encrypts only the key regions in the video, thereby ensuring security while minimizing the impact on coding efficiency. However, existing ROI-based video encryption methods suffer from insufficient flexibility and lack of a unified evaluation system. To address these issues, we propose a visual perception-based tunable framework and evaluation benchmark for H.265/HEVC ROI encryption. Our scheme introduces three key contributions: 1) A ROI region recognition module based on visual perception network is proposed to accurately identify the ROI region in videos. 2) A three-level tunable encryption strategy is implemented while balancing security and real-time performance. 3) A unified ROI encryption evaluation benchmark is developed to provide a standardized quantitative platform for subsequent research. This triple strategy provides new solution and significant unified performance evaluation methods for ROI selective encryption field. Experimental results indicate that the proposed benchmark can comprehensively measure the performance of the ROI selective encryption. Compared to existing ROI encryption algorithms, our proposed enhanced and advanced level encryption exhibit superior performance in multiple performance metrics. In general, the proposed framework effectively meets the privacy protection requirements in H.265/HEVC and provides a reliable solution for secure and efficient processing of sensitive video content.

**Index Terms**—H.265/HEVC, Video Privacy Protection, Visual Perception Network, ROI Selective Encryption, Encryption Evaluation Benchmark.

## I. INTRODUCTION

With the rapid development of video technologies, such as home health monitoring [1], intelligent video surveillance [2], and remote conferencing, video data has become a primary medium for information exchange. Although these video streams provide great convenience and enable intelligent analysis, they often contain a substantial amount of sensitive information, particularly facial features, raising significant privacy concerns. Traditional encryption schemes, such as full-frame encryption, are effective privacy protection solutions. However, such methods completely disrupt the structure and content of the video, making it unsuitable for

This work was supported in part by the National Natural Science Foundation of China under Grant 62202234, 62372128, 62401270, U22B2062, 62172232; China Postdoctoral Science Foundation under Grant 2023M741778; Natural Science Foundation of Guangdong Province under Grant 2023A1515011575; Nanjing Major Science and Technology Special Project under Grant 202405002.

Xiang Zhang, Geng Wu, Wenbin Huang, Daoyong Fu, and Zhangjie Fu are with the Engineering Research Center of Digital Forensics, Ministry of Education, Nanjing University of Information Science and Technology, Nanjing, Jiangsu 210044, China (e-mail: zhangxiang@nuist.edu.cn; 202312490279@nuist.edu.cn; wenbinhuang@nuist.edu.cn; fudymo@hotmail.com; fzj@nuist.edu.cn).

Fei Peng is with the School of Artificial Intelligence, Guangzhou University, Guangzhou, Guangdong 510006, China (e-mail: eepengf@gmail.com).

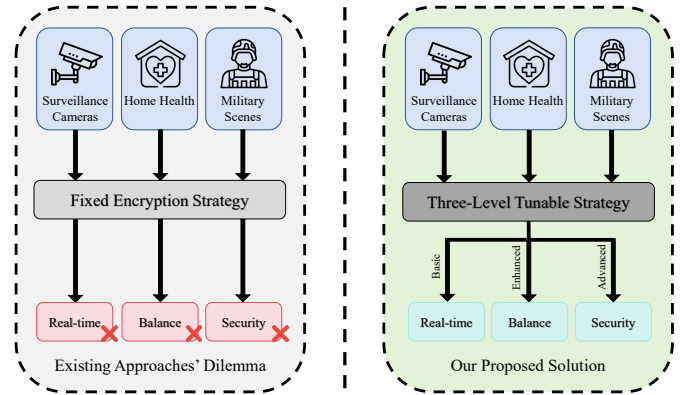


Fig. 1: Comparison between fixed encryption strategy and proposed three-level encryption strategy

any subsequent analysis [3]. Homomorphic encryption allows computation to be performed directly on encrypted data, but its extremely high computational complexity (e.g., exponential operations) makes it impractical for processing high-bitrate video streams in real-time systems [4].

Therefore, protecting sensitive information while maintaining the usability of video data for automated analysis tasks (such as behavior recognition) remains a significant challenge. To address this issue, researchers have proposed Region of Interest (ROI) encryption. The core concept of ROI encryption is to selectively encrypt only sensitive regions within video frames while keeping non-sensitive areas unencrypted. Early naive ROI encryption methods performed encryption directly on raw pixel data prior to compression, severely disrupting the spatial correlations within the video [5]–[9]. As a result, the compression efficiency of subsequent codecs (e.g., H.265/HEVC) was significantly reduced, and bitstream compatibility could no longer be guaranteed [10].

Consequently, Region of Interest (ROI) selective encryption (SE) [11], a strategy that integrates encryption with video encoding, has become a key research focus in the field of video security [12]. Since H.265/HEVC is currently one of the most widely adopted video coding standards [13], ROI SE techniques based on H.265/HEVC have become a major research focus in the field of video encryption [14]–[19]. Such approaches preserve bitstream format compliance with minimal bitrate overhead and enable standard decoders to reconstruct non-ROI regions without requiring access to the encryption key. Despite the great potential of ROI SE based on H.265/HEVC, existing algorithms still face two major challenges: (1) **Lack of flexibility in encryption schemes**: existing methods use a fixed combination of syntax elements

TABLE I SUMMARY OF EVALUATION METRICS IN SOME TYPICAL ROI SE SCHEMES

Author	Standard	Experimental Focus
Peng et al. [14]	H.264/AVC	Key security, Encoding time, Bit rate change
Yu et al. [16]	H.265/HEVC	PSNR, SSIM, IoU, Encoding time
Taha et al. [17]	H.265/HEVC	PSNR, SSIM, Bit rate change, Key security
Sohn et al. [18]	H.264/SVC	Bit rate change
Farajallah et al. [19]	H.265/HEVC	Bit rate change

for encrypting ROI regions. However, as shown in Fig. 1, different application scenarios exhibit diverse requirements for security and real-time performance. Therefore, existing methods struggle to meet diverse needs and fail to achieve a dynamic balance between security and real-time performance.

**(2) Lack of a Unified and Standardized Evaluation Benchmark:** This remains the most critical issue hindering progress in this field. We reviewed some typical ROI encryption studies based on H.264/AVC and H.265/HEVC, and summarized their evaluation systems in Table I. As shown in the table, there is considerable variation in the performance metrics adopted across different studies. Some works primarily focus on efficiency-related indicators, such as encoding time [14], [16], while others emphasize visual quality and bit rate change [17], [19].

This arbitrariness in metric selection, combined with the lack of transparency in testing methodologies, has led to the absence of a unified, comprehensive, and quantifiable benchmarking framework in the field. As a result, the primary issue to be addressed is building a standard evaluation benchmark. Based on this, we propose a visual perception-based tunable framework and evaluation benchmark for H.265/HEVC ROI encryption. Firstly, a visual perception network is used to identify ROI coordinates and segment the video frame into ROI and non-ROI region. Then, a three-level tunable ROI encryption strategy (the basic level, the enhanced level, and the advanced level) is applied to encrypt ROI region of the video based on the user requirements. Finally, a unified ROI encryption evaluation benchmark is developed to better measure the performance of ROI encryption. In summary, the main contributions of this paper are as follows:

- A ROI Region Recognition Module Based on Visual Perception Network.** We propose a ROI region recognition module effectively identify ROI region in video by training a visual perception network, significantly enhancing the accuracy of ROI recognition.
- Three-Level Tunable ROI Selective Encryption Strategy.** We present a three-level tunable ROI selective encryption strategy to balance security and real-time performance. Each level of encryption strategy perturbs different syntax elements. Users can flexibly select the encryption strength according to available device resources.
- A Unified ROI Encryption Evaluation Benchmark.** We pioneer a comprehensive evaluation benchmark which contains the evaluation of ROI region recognition accuracy and ROI region perturbation effect. It enables the quantitative comparison of different ROI selective encryption schemes and provides an important reference for future optimization efforts.
- Extensive Experimental Validation with Different**

**Comparison Algorithms.** We conduct extensive experiments using the proposed ROI encryption evaluation benchmark and compare our method with Start-of-the-Art approaches. The experimental results demonstrate that the proposed scheme effectively satisfies diverse requirements in terms of security and real-time performance.

The remaining content is as follows: Section II presents related work. Section III describes the preliminaries. Section IV details the proposed video encryption scheme. Section V provides the proposed ROI encryption evaluation benchmark. Section VI introduces experimental results and analysis. Finally, conclusions are drawn in Section VII.

## II. RELATED WORK

### A. ROI Naive Encryption

In ROI naive encryption, the ROI within the video is separately extracted and treated as the key region that needs to be protected. Traditional encryption algorithms, such as the Advanced Encryption Standard (AES), are usually applied to encrypt the data within this region. Carrillo *et al.* [5] proposed protecting the ROI by encrypting the macroblock in the ROI before compression. However, this encryption process results in an approximately 23% increase in video bit rate. Dufaux *et al.* [6] introduced a privacy protection method for video surveillance, utilizing a random permutation method to pseudo-randomly permute the alternating current (AC) coefficients within the ROI block. This algorithm also leads to a significant increase in bit rate.

To address the bit rate increment issue, Dufaux *et al.* [7] proposed randomly selecting portions of the video bitstream for pseudo-random inversion, achieving a zero bit rate increase. However, this method compromises the compatibility of the video encoding format, leading to video decoding failure. Hosny *et al.* [8] suggested a privacy protection approach for surveillance videos. They use YOLOv3 to detect the face region, then encrypting each pixel within the extracted ROI. This method does not fully obfuscate the original data, allowing attackers to potentially recover sensitive information. Li *et al.* [9] proposed the PPL-enc scheme, which uses SOLOv2 to accurately identify privacy regions and combines pixel-level encryption with attribute-based encryption. This scheme also offers good real-time performance with minimal impact on storage and transmission.

Although ROI naive encryption can protect privacy by directly encrypting sensitive regions, it faces several technical challenges of a significant decrease in video coding efficiency, with bit rate increases ranging from 8% to 23%, Therefore, ROI selective encryption is proposed to solve the problems.

### B. ROI Selective Encryption

Selective encryption takes into account both security and efficiency and has become a research focus in the field of video privacy protection. Peng *et al.* [14] proposed a solution based on Flexible Macroblock Ordering (FMO) and chaotic encryption. FMO is first used to map the face region to a specific slice group, and then the chaotic encryption algorithm

is used to encrypt the region. This method achieves a certain balance between security and encryption efficiency. However, the division of FMO slice groups may cause the encrypted region to exceed the ROI range. Im *et al.* [15] combined Mask Region-Based Convolutional Neural Network (Mask R-CNN) object detection and Context-Adaptive Binary Arithmetic Coding (CABAC) to encrypt the detected privacy region, which not only ensures the precise positioning of the ROI, but also maintains the compatibility of the coding process. However, some ROI information may not be fully encrypted in low-bitrate videos.

To solve the above problems, Yu *et al.* [16] proposed a coding unit (CU) level ROI encryption scheme based on H.265/HEVC. By using YOLOv4 [20] to detect the face region and selectively encrypt the corresponding CU, it achieved relatively accurate ROI protection. However, it will cause the problem of reduced compression efficiency in high-resolution videos. Taha *et al.* [17] adopted a tile-level encryption strategy, using the independence of tiles in H.265/HEVC to encrypt only the key syntax elements in the tile containing the ROI, thereby achieving real-time protection. However, the limitations of tile division may cause the encrypted region to deviate from the actual ROI. Sohn *et al.* [18] divided the face region into foreground and background based on scalable video coding technology, and adopted an encryption method of randomly flipping the transform coefficient sign for the foreground region. It has shortcomings in encryption propagation control. The AES-based scheme proposed by Farajallah *et al.* [19] adopts full encryption and selective encryption strategies respectively. Selective encryption shows good format compatibility and encryption efficiency by encrypting only the key syntax elements in CABAC encoding, but it still has limitations in the precise control of the ROI region.

### C. ROI Region Recognition

Both ROI naive encryption and ROI selective encryption rely on the accurate identification and effective extraction of the ROI, making the precision of the ROI region recognition technology crucial. Early ROI encryption schemes predominantly relied on traditional ROI region recognition methods, such as face detection based on skin color models or using the OpenCV library [21]. These methods identify ROI regions through color space conversion and feature matching, offering advantages in terms of low computational complexity. However, detection accuracy decreases significantly when encountering challenges such as lighting variations, object occlusion, or overlapping objects [22]. Additionally, these methods have difficulty adapting to morphological changes in the object, which can lead to a mismatch between the encrypted region and the actual sensitive region.

In recent years, deep learning-based ROI region recognition technology has gradually become the dominant choice in ROI encryption due to its high-precision detection capabilities. He *et al.* [23] proposed Mask R-CNN. It is a two-stage ROI region recognition algorithm that combines object detection and instance segmentation. It excels in accurately capturing the contours of objects, making it particularly suitable for privacy

regions with irregular shapes. However, its computational complexity is high, which may hinder the efficiency of real-time encryption. Wang *et al.* [24] proposed SOLOv2, which is an instance segmentation-based ROI region recognition model, achieves efficient object segmentation through dynamic convolution and mask prediction. It significantly reduces computational complexity while maintaining high accuracy, making it suitable for real-time ROI encryption in high-resolution videos. Redmon *et al.* [25] proposed YOLOv3, which is a single-stage ROI region recognition algorithm with high speed and real-time performance. By incorporating multi-scale prediction and feature pyramid network, YOLOv3 improves detection accuracy for small and dense objects. However, YOLOv3 is slightly less accurate than two-stage detection algorithms, which may cause the encrypted region to slightly exceed the actual sensitive ROI region.

## III. PRELIMINARIES

### A. Object Detection Based on Visual Perception Network

Object detection technology plays a crucial role in video content analysis and encryption systems. To maintain both high detection accuracy and real-time performance, we employ a visual perception network to accurately extract sensitive regions, providing reliable input for subsequent ROI encryption. The architecture of this network is illustrated in Fig. 2.

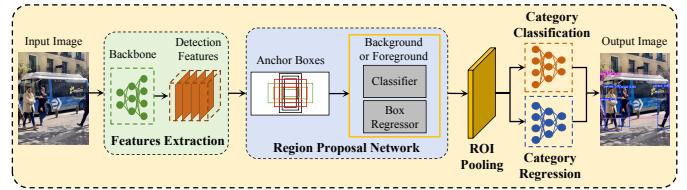


Fig. 2: The architecture of visual perception network

The visual perception network first utilizes backbone to extract detection features from the input image. Backbone consists of multiple convolutional and pooling layers, enabling the network to capture both local and global features, thus generating high-dimensional feature maps [26]. The detection features are then input into Region Proposal Network (RPN) [27] to generate multiple anchor boxes through a sliding window mechanism. These anchor boxes vary in scale and aspect ratio, enabling the network to accommodate objects of different sizes and shapes. Afterwards, the multiple anchor boxes are input into a foreground-background classifier and box regressor. Among them, the foreground-background classifier is used to determine whether the anchor box is a foreground (object) or a background and its loss function is:

$$L_{\text{cls}}^{\text{RPN}} = -\frac{1}{N} \sum_{i=1}^N [p_i \log \hat{p}_i + (1 - p_i) \log (1 - \hat{p}_i)], \quad (1)$$

where  $N$  is the number of anchor boxes,  $p_i$  is the true label of anchor box  $i$  (1 for foreground, 0 for background), and  $\hat{p}_i$  is the probability predicted by RPN that anchor box  $i$  corresponds to the foreground. while the foreground-background box regressor is used to fine-tune the position of the anchor

box in order to generate more accurate candidate regions and its loss function is:

$$L_{\text{reg}}^{\text{RPN}} = \frac{1}{N} \sum_{i=1}^N \text{smooth}_{L1}(t_i - \hat{t}_i), \quad (2)$$

where  $t_i$  is the true offset of anchor box  $i$ ,  $\hat{t}_i$  is the offset of anchor box  $i$  predicted by RPN, and  $\text{smooth}_{L1}(\cdot)$  is the smooth L1 loss function. Through the above process, RPN generates a series of high-quality candidate regions. Then, the ROI pooling layer maps the candidate regions into a fixed-size classification vector. Finally, the classification vector is entered into category classification network and category regression network. Among them, category classification network classifies the classification vector to determine which category it belongs to and its loss function is:

$$L_{\text{cls}} = -\frac{1}{M} \sum_{j=1}^M \log \hat{p}_{j,c_j}, \quad (3)$$

where  $M$  is the number of ROIs,  $c_j$  is the true category of ROI  $j$ , and  $\hat{p}_{j,c_j}$  is the probability that ROI  $j$  belongs to category  $c_j$ . While category regression network is used to fine-tune the position of the classified ROI to generate a more accurate bounding box. The category regression loss is:

$$L_{\text{reg}} = \frac{1}{M} \sum_{j=1}^M \text{smooth}_{L1}(t_j - \hat{t}_j), \quad (4)$$

where  $t_j$  is the actual offset of ROI  $j$ , and  $\hat{t}_j$  is the offset predicted by the category regression network.

Through the features extraction, region proposal network, ROI pooling, category classification and regression, the visual perception network accurately extracts sensitive regions from the image, enabling reliable input for the tunable ROI encryption process.

### B. Analysis of Syntax Elements in H.265/HEVC

The syntax elements is the basic units used to represent video information during the encoding process. In H.265/HEVC, the video frame is compressed into a bitstream after prediction, transformation, quantization and entropy coding. In this process, a large number of syntax elements are obtained. TABLE II provides the main syntax elements in H.265/HEVC. These syntax elements are binarized using three methods:  $k$ -order Exponential Golomb ( $EG_k$ ) coding,  $k$ -order Truncated Rice ( $TR_k$ ) coding, and Fixed-Length (FL) coding [28]. After the binarization stage, CABAC is applied. H.265/HEVC has two entropy coding modes in CABAC: regular mode and bypass mode. In the regular mode, the encoding of each binary value is based on an adaptively updated probability model. In the bypass mode, the encoding of syntax elements is based on fixed probabilities [29].

While encrypting the syntax elements in regular mode will inevitably result in a change in the bit rate, and encrypting syntax elements in bypass mode will not increase the bit rate [30]. Based on this, we analyze the impact of encryption of each syntax element below.

TABLE II MAIN SYNTAX ELEMENTS OF H.265/HEVC

Syntax element	Entropy mode	Binarization	Category
Luma IPM	Regular	$TR_k$	Prediction
Chroma IPM	Regular	$TR_k$	
Merge index	Regular, Bypass	FL	
MVD sign	Bypass	FL	
MVD value	Bypass	$EG_k$	
MVPIIdx	Regular	FL	
RefFrmIdx	Regular, Bypass	$EG_k$	
Residual sign	Bypass	FL	Residual
Residual value	Bypass	$TR_k$	
Delta QP value	Regular, Bypass	$EG_k$	
SAO parameter	Bypass	$EG_k$	Filtering

As shown in TABLE II, syntax elements are divided into three categories: prediction, residual, and filtering. In video coding, decoded pixels are primarily restored by prediction and residual data. Thus, encrypting prediction and residual syntax elements will cause a strong perturbation effect [10]. Furthermore, according to the analysis in [31], SAO parameters do not significantly contribute to visual distortion. To enhance efficiency, it is recommended not to encrypt these parameters.

In conclusion, encrypting IPM, MVD, Residual, and Delta QP offers a higher scrambling effect, and encrypting IPM, Merge index, MVPIIdx, RefFrmIdx, and Delta QP inevitably change the bit rate. Additionally, the encryption must strictly adhere to the encoding rules of syntax elements to ensure that the encrypted bitstream remains compatible with the H.265/HEVC format.

## IV. PROPOSED THREE-LEVEL TUNABLE ROI SELECTIVE ENCRYPTION SCHEME FOR H.265/HEVC

Based on the characteristics of syntax elements, we propose a graded encryption strategy for H.265/HEVC with three levels of encryption, including basic level, enhanced level, and advanced level. This strategy allows for flexible selection of different encryption methods for ROI regions according to specific needs. The complete framework of the proposed three-level encryption strategy is shown in Fig. 3, which consists of two core components: ROI region recognition module and three-level tunable ROI selective encryption.

### A. ROI Region Recognition Module

In the ROI recognition process, we treat “face” as the target and the recognition process is as follows:

$$\text{ROI\_Coords} = \text{VPN}(F_n), \quad (5)$$

where  $F_n$  represents the current input frame,  $\text{VPN}(\cdot)$  represents a pre-trained object detection model based on visual perception network which is described in Section III-A.  $\text{ROI\_Coords}$  is the output of the model, which is the ROI coordinate file.

Upon detection,  $\text{ROI\_Coords}$  is stored as text coordinates in the format  $\text{frameID} : [i, (x_1^i, y_1^i, x_2^i, y_2^i)]$ , where  $i$  denotes the frame index, and  $(x_1^i, y_1^i)$  and  $(x_2^i, y_2^i)$  represent the pixel coordinates of the top-left and bottom-right corners of the

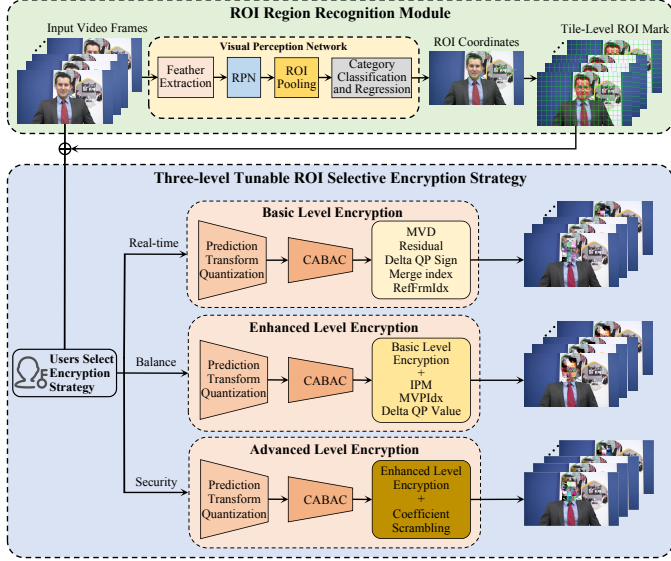


Fig. 3: The proposed three-level encryption strategy

ROI region in the  $i^{th}$  frame, respectively. Then, we classify Tiles in each frame into ROI Tiles and non-ROI Tiles based on ROI\_Coords. Afterwards, the encoder configuration file is modified to enable Tile partition, configured in a fixed-size mode with a uniform Tile size of  $32 \times 32$ . The classification of Tiles is expressed as:

$$\text{curTile} = \begin{cases} \text{ROI-Tile}, & \text{if } \text{mark}(\text{curTile}) = 1 \\ \text{nonROI-Tile}, & \text{otherwise,} \end{cases} \quad (6)$$

where  $\text{mark}(\cdot)$  function evaluates whether the current Tile's coordinate range overlaps with the ROI\_Coords, returning a Boolean value according to the following formula:

$$\text{mark}(\text{curTile}) = \begin{cases} 1, & \text{if } (x_{1\_tile}^i, y_{1\_tile}^i, x_{2\_tile}^i, y_{2\_tile}^i) \\ & \cap (x_1^i, y_1^i, x_2^i, y_2^i) \neq \emptyset \\ 0, & \text{otherwise,} \end{cases} \quad (7)$$

where  $(x_{1\_tile}^i, y_{1\_tile}^i, x_{2\_tile}^i, y_{2\_tile}^i)$  denotes the boundary coordinates of the current Tile in the  $i^{th}$  frame, and  $\cap$  is the intersection sign. After classifying all tiles, we proceed with encrypting the video frames. If the currently Tile is an ROI-Tile, the proposed three-level ROI selective encryption strategy is applied to the CUs within the Tile. Otherwise, the current Tile is encoded normally.

### B. Three-level Tunable ROI Selective Encryption

In our strategy, a binary key generation method based on Advanced Stream Encryption-Counter Mode (ASE-CTR) [32] is first employed to generate the binary key stream  $S$ :

$$S = \text{ASE}(K, \text{CTR}), \quad (8)$$

where  $\text{ASE}(K, \text{CTR})$  represents the pseudo-random binary key stream generated by encrypting with  $K$  and counter CTR, the counter CTR is incremented after encrypting each syntax element to ensure that the key stream for each syntax element is unique. After generating the binary key stream sequence

$S = \{s_1, s_2, \dots, s_{kl}\}$ , where  $kl$  is the length of  $S$ , it is used to encrypt the binarized syntax elements in each CU of ROI-Tile, which is identified in Section IV-A. The following section provides a detailed introduction to the three-level tunable ROI selective encryption strategy.

**1) Basic Level Encryption:** The basic level encryption aims to ensure real-time performance and zero bit increment during encoding, while providing basic visual distortion effects. It is suitable for scenarios with high real-time requirements. This strategy involves encrypting certain syntax elements such as MVD sign and value, residual sign and value, the suffix of Delta QP, Merge index in bypass mode, and the suffix of RefRmIdx in bypass mode. The specific encryption methods for these syntax elements are described below.

**Encryption of MVD Sign and Value.** MVD represents the difference between the motion vector of the current prediction unit and its predicted value, comprising horizontal and vertical components, each consisting of a sign and a value. These components are encoded separately. The signs are binarized using FL coding and encrypted as:

$$\text{encMVDHsign} = \text{MVDHsign} \oplus s_i, \quad 0 \leq s_i \leq 1, \quad (9)$$

$$\text{encMVDVsign} = \text{MVDVsign} \oplus s_i, \quad 0 \leq s_i \leq 1, \quad (10)$$

where  $\text{MVDHsign}$  and  $\text{MVDVsign}$  are the signs of the horizontal and vertical components of current MVD, respectively.  $s_i$  is encryption key extracted from  $S$ . While MVD value is binarized using EG<sub>1</sub> and its suffix is encrypted as:

$$\text{encMVDsuffix} = \text{MVDsuffix} \oplus s_i, \quad 0 \leq s_i \leq 1. \quad (11)$$

**Encryption of Residual Sign and Value.** The residual structure is similar to MVD, consisting of a sign and a value, which are also encoded separately. The sign  $\text{CoefSign}$  of each non-zero coefficient is encoded independently into the bitstream. Here,  $\text{CoefSign} = 0$  indicates a positive number, and  $\text{CoefSign} = 1$  indicates a negative number.  $\text{CoefSign}$  is binarized using FL coding and encrypted as:

$$\text{encCoefSign} = \text{CoefSign} \oplus s_i, \quad 0 \leq s_i \leq 1. \quad (12)$$

The residual value  $\text{absCoefLevel}$  consists of two parts:  $\text{CoefbaseLevel}$  and  $\text{CoefremainingLevel}$ .  $\text{CoefbaseLevel}$  is not encrypted since it is encoded by regular mode. While  $\text{CoefremainingLevel}$  is binarized using TR<sub>k</sub> and encoded by bypass mode. As a result, its suffix  $\text{Coefsuffix}$  is encrypted as:

$$\text{encCoefsuffix} = \text{Coefsuffix} \oplus s_i, \quad 0 \leq s_i \leq 1. \quad (13)$$

**Encryption of Delta QP sign.** The quantization parameter (QP) controls the compression quality and encoding bit rate. It is composed of a sign and a value. To maintain a consistent bit rate, only the sign  $\text{uiSign}$  is selected for encryption. If  $\text{uiSign} = 0$ , the Delta QP is positive. If  $\text{uiSign} = 1$ , the Delta QP is negative.  $\text{uiSign}$  is encrypted as:

$$\text{encuiSign} = \text{uiSign} \oplus s_i, \quad 0 \leq s_i \leq 1. \quad (14)$$

**Encryption of Merge index.** The merge mode is used for inter prediction. In inter prediction, a candidate motion vector reference list of length 5 is constructed directly from adjacent

prediction units. The index number within this list is referred to as the Merge index, and its value ranges from 0 to 4. The Merge index is encoded using FL coding and encrypted as:

$$encUnaryIdx = (UnaryIdx + s_i) \% 5, \quad 0 \leq s_i \leq 3. \quad (15)$$

**Encryption of ReffRmIdx.** In H.265/HEVC, the current frame predicts its content by reference frames. The encoder uses reference frame index to represent each reference frame. We encrypt the suffix of reference frame index since it is binarized using  $EG_k$  and encoded by bypass mode. However, the upper limit of the reference frame index varies depending on the buffer. Therefore, the encryption of the reference frame index suffix  $RFIS$  according to the current number of the frames in the buffer  $RN$  with the maximal value 4 is:

$$encRFIS = \begin{cases} RFIS \oplus s_i, & 0 \leq s_i \leq 1, \text{ if } RN = 2 \\ (RFIS + s_i) \% 3, & 0 \leq s_i \leq 1, \text{ if } RN = 3 \\ RFIS \oplus s_i, & 0 \leq s_i \leq 3, \text{ if } RN = 4. \end{cases} \quad (16)$$

2) *Enhanced Level Encryption:* The enhanced level encryption preserves the real-time advantages of basic level encryption while strengthening content protection by broadening the scope of encryption. Building on the basic level encryption, the enhanced level encryption includes the encryption of IPM, MVPIdx, and Delta QP value, which can produce significant visual disruption effects. Since the entropy coding mode for these elements is regular mode, inevitably resulting in an increase in the bit rate. The specific encryption methods for these syntax elements are described below.

**Encryption of Luma IPM.** Luma IPM is a critical syntax element in H.265/HEVC. The total number of luma IPMs is 35. During the encoding process, a list contains three Most Probable Modes (MPMs) is first constructed. If the current luma IPM is in the list, a MPM index  $MPMIdx$  is recorded.  $MPMIdx$  is encoded by bypass mode and encrypted as:

$$encMPMIdx = (MPMIdx + s_i) \% 3, \quad 0 \leq s_i \leq 3. \quad (17)$$

If the current luma IPM is not included in the MPMs list, the remaining 32 modes will be conveniently represented by a 5-bit codeword  $LumaIPM$  and then encrypted as:

$$encLumaIPM = LumaIPM \oplus s_i, \quad 0 \leq s_i \leq 31. \quad (18)$$

**Encryption of Chroma IPM.** Chroma IPM has five prediction modes, and is recorded using the chroma IPM index  $ChromaIPM$ . The encryption of  $ChromaIPM$  can significantly perturb the video. Therefore, we encrypt it as:

$$encChromaIPM = (ChromaIPM + s_i) \% 3, \quad 0 \leq s_i \leq 3. \quad (19)$$

**Encryption of MVPIdx.** MVP index is the syntax element in the Advanced Motion Vector Prediction (AMVP). When the AMVP mode is used, the motion vector is predicted from neighbor blocks, and a list of MVP candidates with a length of 2 is formed. The MVP index  $MVPIdx$ , that identifies the optimal MVP from this list, is binarized by regular mode and encrypted as:

$$encMVPIdx = MVPIdx \oplus s_i, \quad 0 \leq s_i \leq 1. \quad (20)$$

**Encryption of Delta QP Value.** To avoid decoding failure, encryption is Delta QP Value  $DQP$  requires ensuring that the encrypted value does not exceed maximum Delta QP value  $MaxDQP$ . The encryption process for  $DQP$  is defined as:

$$encDQP = (DQP \oplus s_i) \% MaxDQP + 1, \quad 0 \leq s_i \leq MaxDQP - 1. \quad (21)$$

3) *Advanced Level Encryption:* The edge region contains the highest concentration of video frame information, making its protection essential [33]. Existing ROI encryption schemes typically perturb syntax elements but neglect edge information. To address this, we proposed an improved coefficient scrambling algorithm based on [34] for edge region in the advanced level encryption, building upon the enhanced level encryption. The brief steps of the coefficient scrambling algorithm are as follows:

Step 1: The Canny operator  $Canny(\cdot)$  is applied to filter the luma component of a frame  $FL$  to obtain the pixel edge information  $FL^{edge}(x, y)$ :

$$FL^{edge}(x, y) = Canny(FL(x, y)). \quad (22)$$

Step 2: The pixel edge information  $FL^{edge}$  is binarized using the binarization function  $Bin(\cdot)$ , resulting in the luma edge binary image  $FL^{bin}$ :

$$FL^{bin}(x, y) = Bin(FL^{edge}(x, y)). \quad (23)$$

Step 3: The TUs in  $FL_n^{bin}$  are classified into two categories based on the pixels  $FL_{TU}^{bin}(x, y)$  in the TUs:

$$TU = \begin{cases} \text{edgeTU}, & \text{if } \sum FL_{TU}^{bin}(x, y) \neq 0 \\ \text{non-edgeTU}, & \text{otherwise.} \end{cases} \quad (24)$$

Step 4: The  $N_{nz}$  non-zero coefficients in an edgeTU are divided into two sets: the first  $N_{nz} - 1$  non-zero coefficients in scan order form the permuted set  $C_{\text{permute}}$ , and the last non-zero scanned coefficient is reserved as  $LastCoef$  for reversible embedding in Step 5. To enhance security beyond the general-purpose generator in [34], a key-driven chaotic permutation is applied to  $C_{\text{permute}}$ . The procedure is as follows:

- 1) Let  $N_p = N_{nz} - 1$  be the number of coefficients to permute. If  $N_p \leq 1$ , skip this step.
- 2) Use the secret key  $K_c$  to generate the initial value  $x_0$  and control parameter  $r$  for a Logistic chaotic map:

$$x_{i+1} = r \cdot x_i (1 - x_i). \quad (25)$$

- 3) Iterate the chaotic map  $N_p$  times to obtain a floating-point sequence  $S = \{x_1, \dots, x_{N_p}\}$ .
- 4) Generate a permutation map  $\pi = \{\pi(1), \dots, \pi(N_p)\}$  by sorting  $S$  and recording the indices.
- 5) Scramble the coefficients in  $C_{\text{permute}} = \{c_1, \dots, c_{N_p}\}$  according to  $\pi$  to obtain the scrambled set  $C'_{\text{permute}} = \{c'_1, \dots, c'_{N_p}\}$ :

$$c'_{\pi(k)} = c_k, \quad k = 1, \dots, N_p. \quad (26)$$

*Step 5:* Reversibly embed the sign into the last non-zero scanned coefficient *LastCoef* in the current TU, as shown below:

$$\text{LastCoef}' = \begin{cases} 2 \times \text{LastCoef} - w, & \text{if } \text{LastCoef} > 0 \\ 2 \times \text{LastCoef} + w, & \text{if } \text{LastCoef} < 0, \end{cases} \quad (27)$$

where  $w$  is a value used to record the TU type. If current TU is edgeTU, set  $w = 1$ . Otherwise, set  $w = 0$ .

## V. ROI ENCRYPTION EVALUATION BENCHMARK

ROI encryption have recently garnered significant attention in the field of video encryption. However, the current research on ROI encryption often lacks comprehensive experimental evaluation, and the measurement indicators used are not standardized. For instance, Peng [14] assessed encoding time and compression ratio. Yu [16] focused on testing the IoU between the encrypted region and the ground truth, as well as encryption time. Taha [17] evaluated their scheme by testing bit rate change, PSNR and SSIM values. These evaluation methods are relatively simplistic, lacking sufficient persuasive power to demonstrate the superiority of the scheme. Furthermore, the inconsistency in measurement indicators complicates effective horizontal comparisons and comprehensive evaluations between different schemes.

To address this issue, We pioneer a new comprehensive **ROI encryption evaluation benchmark** to provide a standardized evaluation platform for different ROI encryption algorithms. We believe that the performance of a ROI encryption algorithm depends on two key factors: First, the IoU between the encrypted regions and the detected ROIs is used to quantify how accurately sensitive areas are covered by the encryption. Secondly, the perturbation effect within the extracted ROI regions, which affects whether the content in these regions is sufficiently perturbed to become unrecognizable. They are the two parts of the proposed benchmark: the evaluation of ROI encryption fineness and ROI region perturbation effect.

### A. The Evaluation of ROI Encryption Fineness

In this section, we evaluate the fineness of ROI encryption at the pixel level. Specifically, the actually encrypted regions of encoded video and the ROI region ground truth are represented as pixel sets, denoted as  $E$  and  $G$ , respectively, where  $E$  represents the set of encrypted pixels and  $G$  represents the set of ROI region ground truth pixels. The encryption fineness is measured using the IoU between these two sets, defined as:

$$\text{IoU} = \frac{|E \cap G|}{|E \cup G|}, \quad (28)$$

where  $|E \cap G|$  denotes the number of pixels in the intersection of the encrypted and ground truth, and  $|E \cup G|$  denotes the number of pixels in their union. The closer the IoU value is to 1, the higher the overlap between the encrypted region and the ground truth, indicating that the encryption covers the sensitive areas more precisely and achieves higher fineness. Conversely, a lower IoU value indicates incomplete or excessive encryption, reflecting insufficient fineness.

To provide a comprehensive assessment for an entire video sequence, the IoU can be computed for each frame and averaged over all frames to obtain the average encryption fineness, denoted as  $\text{IoU}_{\text{avg}}$ :

$$\text{IoU}_{\text{avg}} = \frac{1}{N} \sum_{i=1}^N \frac{|E_i \cap G_i|}{|E_i \cup G_i|}, \quad (29)$$

where  $N$  is the total number of frames in a video, and  $E_i$  and  $G_i$  represent the encrypted pixel set and ground truth pixel set in the  $i$ -th frame, respectively. This metric quantifies the pixel-level coverage precision of the encrypted regions and provides a unified and intuitive standard for evaluating the fineness of ROI encryption algorithms.

### B. The Evaluation of ROI Region Perturbation Effect

The evaluation of ROI region perturbation effect includes two parts: the analysis of subjective vision and the analysis of objective indicators.

1) *Analysis of Subjective Vision:* To assess the perceptual impact of encryption on the ROI region, we conduct subjective vision comparison by presenting encrypted video frames to the observers. This leverages participant feedback to evaluate the level of perturbation in the ROI region. Specifically, at least two video sequences with different resolutions and texture complexities are selected. For each video sequence, we choose the first and last frames, and show their original frames, encrypted frames (the proposed algorithm), and the corresponding decrypted frames (the proposed algorithm), which can refer to Fig. 5. Subsequently, the whole encrypted frames, encrypted images of ROI region, and encrypted edge images of ROI region are compared with those produced by State-of-the-Art algorithms, which can refer to Fig. 7, Fig. 8, and Fig. 9. Furthermore, various subjective and intuitive visualization examples can be included in the future to illustrate the encryption effectiveness of the proposed algorithm.

2) *Analysis of Objective Indicators:* Unlike global encryption algorithms, evaluating an ROI encryption algorithm presents unique challenges, as it encrypts only the ROI region of a video frame, and the extracted ROI region may vary across different algorithms. Consequently, the objective indicators used for global encryption cannot be directly applied. To address this issue, we designed an accurate ROI region extraction criterion. This criterion enables precise extracting of all ROI regions based on different ROI region recognition algorithms. Subsequently, we apply various objective evaluation indicators to these regions to assess the security of the encryption algorithm.

**ROI Region Extraction Criterion.** In video coding standards, video data are typically compressed at the level of coding units rather than individual pixels. Therefore, to accurately assess the perturbation effect within the ROI region, evaluation metrics should be applied to the actual coding units that have been encrypted. To this end, we propose an ROI region extraction criterion based on basic coding units, enabling precise identification of all encrypted units and ensuring that the evaluation results correspond strictly to the actual encrypted regions.

*a) Definition of Basic Coding Unit:* We first define  $U$  as a “basic coding unit” in video coding. The basic coding unit is a general concept, but its specific form varies across different video coding standards. For instance, it corresponds to a Macroblock (MB) in H.264/AVC and to a Coding Unit (CU) in H.265/HEVC.

*b) Identification of Target Unit Set:* For any video frame, let  $S_{\text{all}}$  denote the set of all basic coding units in the frame:

$$S_{\text{all}} = \{U_1, U_2, \dots, U_n\}, \quad (30)$$

where  $n$  is the total number of basic coding units in the frame. Given the ROI coordinates  $ROI\_Coords$  output by the ROI recognition module, the encoder first traverses  $S_{\text{all}}$ , if the current basic coding unit  $U_j$  overlaps with the ROI region, it is marked as a ROI basic coding unit. All marked ROI basic coding units form the ROI unit set  $S_{\text{ROI}}$ :

$$S_{\text{ROI}} = \{U_j \in S_{\text{all}} \mid \text{Area}(U_j) \cap \text{Area}(ROI\_Coords) \neq \emptyset\}. \quad (31)$$

where  $\text{Area}(\cdot)$  denotes a function that returns pixel coordinate sets. The intersection operator  $\cap$  returns the same pixel coordinates between these pixel coordinate sets, and  $\emptyset$  represents an empty set.

*c) Data Extraction:* To compute objective evaluation metrics, two types of data are extracted according to  $S_{\text{ROI}}$ :

- $D_{\text{ori}}(U_j)$ : Y, U, V components of  $U_j$  of the original video in  $S_{\text{ROI}}$ .
- $D_{\text{enc}}(U_j)$ : Y, U, V components of  $U_j$  of the encrypted video in  $S_{\text{ROI}}$ .

These data are aggregated to form the original ROI pixel set  $P_{\text{ori}}$  and the encrypted ROI pixel set  $P_{\text{enc}}$ :

$$P_{\text{ori}} = \bigcup_{U_j \in S_{\text{ROI}}} D_{\text{ori}}(U_j), \quad P_{\text{enc}} = \bigcup_{U_j \in S_{\text{ROI}}} D_{\text{enc}}(U_j). \quad (32)$$

where the symbol  $\bigcup$  denotes the union of sets, which combines the Y, U, and V components into a complete ROI pixel set.

Finally, all objective evaluation metrics are computed by comparing  $P_{\text{ori}}$  and  $P_{\text{enc}}$ . By adopting the above ROI region extraction criterion, the data used for assessment strictly correspond to the actual encrypted ROI regions. Therefore, the evaluation results are significantly more accurate and reliable.

**Objective Evaluation Indicators.** After extracting the ROI region of each frame based on the proposed ROI region extraction criterion, we can integrate a comprehensive set of objective evaluation indicators to systematically assess the perturbation effect of ROI region. These indicators include: Peak Signal-to-Noise Ratio (PSNR), Structural Similarity Index (SSIM), Edge Difference Ratio (EDR), information entropy, Pixel Change Rate (NPCR), Unified Average Change Intensity (UACI), and Bit Rate Change. To provide a clear overview, Table III summarizes the key objective indicators along with their calculation formulas and evaluation dimensions. The following provides a detailed interpretation of the indicators.

PSNR is a commonly used video quality evaluation metric. It quantifies the degree of video distortion by calculating the difference between the original video and the encrypted video. The lower the PSNR, the higher the security of the encrypted video. In the formula, Mean Squared Error (MSE) is the

average pixel difference between the original and encrypted video frame, calculated as:

$$\text{MSE} = \frac{1}{N} \sum_{i=1}^N (I_{\text{ori}}(i, j) - I_{\text{enc}}(i, j))^2, \quad (33)$$

where  $I_{\text{ori}}(i, j)$  and  $I_{\text{enc}}(i, j)$  are the pixel values at position  $(i, j)$  for the original and encrypted video frame, respectively, and  $N$  is the total number of pixels in the video frame.

SSIM is a metric used to measure the similarity between video frames. It comprehensively evaluates the similarity of video frames from three aspects: brightness, contrast, and structure. The smaller the value of SSIM, the greater the difference between two video frames. In the formula,  $\mu_1$  and  $\mu_2$  are the average luminance of the original video frame and the encrypted video frame,  $\sigma_1^2$  and  $\sigma_2^2$  are the variances of the original video frame and the encrypted video frame, used to measure the contrast of the video frames.  $\sigma_1\sigma_2$  is the covariance between the original video frame and the encrypted video frame.  $c_1$  and  $c_2$  are the constants.

EDR is an important indicator to evaluate edge distortion of video encryption algorithms. The edge information of the encrypted video frame should be severely distorted so that it cannot be recognized. The higher the EDR value, the greater the edge distortion. In the formula,  $PE(i, j)$  and  $CE(i, j)$  are the edge pixel value of the original video frame and the encrypted video frame at position  $(i, j)$ , respectively, and  $h$  and  $w$  are the height and width of the video frame.

Information entropy is used to measure the randomness and uncertainty of encrypted video. The closer the information entropy value is to the ideal value of 8, the stronger the randomness and uncertainty of the encrypted video. In the formula,  $L$  represents the binary representation length of the pixel value, and  $p(I_j)$  is the probability of the pixel value  $I_j$  appearing.

NPCR and UACI are two commonly used indicators for evaluating the ability of encryption schemes to resist differential attacks. The expected value of NPCR and UACI are 99.6094% and 33.4635%, respectively. In the formula of NPCR,  $D(i, j)$  is the difference matrix, defined as:

$$D(i, j) = \begin{cases} 0, & \text{if } C_1(i, j) = C_2(i, j) \\ 1, & \text{if } C_1(i, j) \neq C_2(i, j), \end{cases} \quad (34)$$

where  $C_1(i, j)$  and  $C_2(i, j)$  represent the encrypted pixel value of two encrypted frame at position  $(i, j)$ .

Bit rate change is an important indicator to measure the encryption algorithm. Ideally, encryption will not cause an increase in bit rate. In the formula,  $\text{Bitrate}_{\text{ori}}$  and  $\text{Bitrate}_{\text{enc}}$  are the bit rates before and after encryption.

In summary, the objective indicators in the proposed benchmark measure the performance in terms of video quality, security strength, and compression efficiency, helping researchers effectively identify the advantages and disadvantages of various ROI encryption schemes on a standardized platform. In the future, more objective indicators can be added to enrich the proposed benchmark.

TABLE III VIDEO ENCRYPTION OBJECTIVE EVALUATION INDICATORS

Indicator	Brief Description	Calculation Formula	Evaluation Dimension
PSNR	Measure pixel-level noise of original and encrypted videos.	$PSNR = 20 \log_{10} \left( \frac{255}{MSE} \right)$	Video Quality
SSIM	Evaluate structural similarity, taking into account brightness and contrast.	$SSIM = \frac{(2\mu_1\mu_2+c_1)(2\sigma_1\sigma_2+c_2)}{(\mu_1^2+\mu_2^2+c_1)(\sigma_1^2+\sigma_2^2+c_2)}$	Video Quality
EDR	Quantify edge distortion introduced by encryption.	$EDR = \frac{\sum_{i=1}^h \sum_{j=1}^w  PE(i,j) - CE(i,j) }{\sum_{i=1}^h \sum_{j=1}^w  PE(i,j) + CE(i,j) }$	Video Quality
Information Entropy	Evaluating the randomness of encrypted data.	$H(I) = -\sum_{j=1}^L p(I_j) \log_2 p(I_j)$	Security Strength
NPCR	Calculate the percentage of pixel change.	$NPCR = \left( \frac{\sum_{i=1}^h \sum_{j=1}^w D(i,j)}{h \times w} \right) \times 100\%$	Security Strength
UACI	Measures the average intensity of pixel differences.	$UACI = \left( \frac{\sum_{i=1}^h \sum_{j=1}^w  C_1(i,j) - C_2(i,j) }{255 \times h \times w} \right) \times 100\%$	Security Strength
Bit rate change	Analyze the change in bit rate after encryption.	$\Delta \text{Bitrate}(\%) = \frac{\text{Bitrate}_{\text{enc}} - \text{Bitrate}_{\text{ori}}}{\text{Bitrate}_{\text{ori}}} \times 100\%$	Compression Efficiency

## VI. EXPERIMENTAL RESULTS AND ANALYSIS

### A. Experimental Setup

The proposed ROI selective encryption scheme is implemented in the H.265/HEVC reference software HM 16.9. The experimental computer configuration is as follows: Intel (R) Core (TM) i7-6700 HQ, 2.6 GHz, 16 GB memory, with Windows 10 operating system, Microsoft Visual Studio 2010, MATLAB 2021a and OpenCV 2.4.7 installed. We use a total of 5 YUV sequences as shown in TABLE IV as our test videos, with resolutions ranging from  $352 \times 288$  to  $2560 \times 1600$ , encoded at a frame rate of 60 fps, using the profile “encoder\_lowdelay\_main”, and the Group of Pictures (GOP) is “IBBB”. The QP is set to 8, 24 and 40 respectively. the visual perception network used in our ROI region recognition module is YOLOv8 [35] in the experiment. The three-level encryption strategy proposed in this paper are compared with two latest H.265/HEVC ROI encryption schemes, including Yu [16] and Taha [17]. we encrypt 50 frames of each sequence by the three schemes for comparison.

TABLE IV YUV TEST SEQUENCE

CLASS	Resolution	Sequence	FPS	Frames
CLASS_A	$352 \times 288$	Akiyo	60	50
CLASS_B	$832 \times 480$	PartyScene	60	50
CLASS_C	$1280 \times 720$	Johnny	60	50
CLASS_D	$1980 \times 1080$	Kimono	60	50
CLASS_E	$2560 \times 1600$	PeopleOnStreet	60	50

To enhance the sensitivity to the face region, the WiderFace dataset is used for targeted training. The dataset contains 32,203 images and 393,703 annotated faces, covering complex scenes such as scale, posture, and occlusion. After training, the output bounding box is strictly focused on the face region. The comparison of detection before and after training is shown in Fig. 4, which clearly shows the significant improvement of the module in face region detection after targeted training, providing high-precision ROI input for subsequent encryption.

### B. Examples

Some sample frames of the proposed three-level encryption strategy on the Akiyo video sequence are shown in Fig. 5.



Fig. 4: Detection results before and after training

Specifically, the frame #1 and #50 of the video sequence are selected to intuitively demonstrate the encryption and decryption effects. The experimental results show that our encryption scheme performs effectively in H.265/HEVC codec. The encrypted frames show severe visual distortion in ROI region, and we can successfully recover the original Akiyo video sequence from the encrypted bitstream.

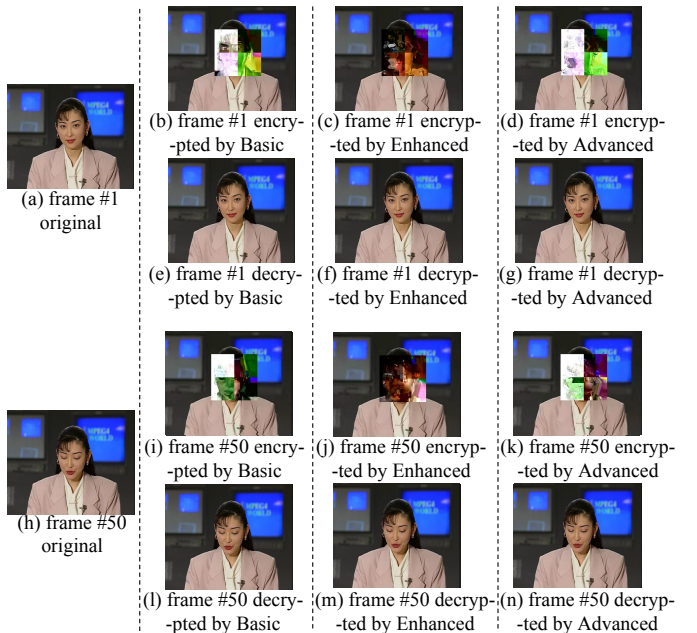


Fig. 5: Some examples of proposed strategy on Akiyo sequence

### C. Performance Analysis

To evaluate the effectiveness of the proposed scheme, this section presents a comprehensive performance analysis conducted based on the proposed benchmark in Section V. The evaluation is structured into two components: ROI region fineness and ROI region perturbation effect.

1) *Comparison of ROI Encryption Fineness*: In this section, we evaluate the fineness of the proposed encryption framework and compare it with only Taha [17], since Yu [16] does not provide its ROI region recognition module. Meanwhile, we use our ROI region recognition module to detect Yu [16] for subsequent comparative experiments. The evaluation is based on  $\text{IoU}_{\text{avg}}$  defined in Section V-A. A higher  $\text{IoU}_{\text{avg}}$  indicates that the encryption scheme can more accurately map the detected ROI into the coding structure, thereby minimizing unnecessary encryption of non-target background pixels.

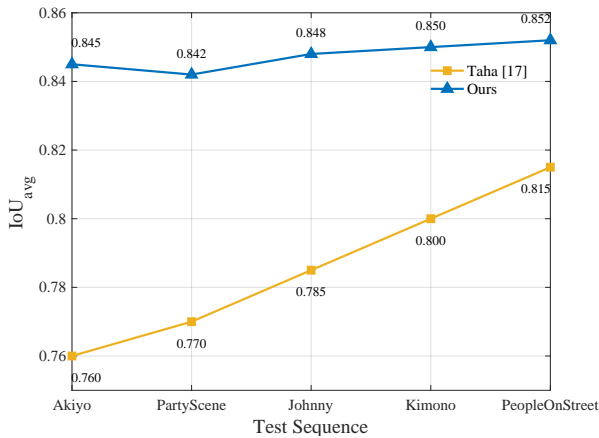


Fig. 6: ROI encryption fineness results

Fig. 6 presents the  $\text{IoU}_{\text{avg}}$  comparison results across all test sequences. As shown in the figure, our scheme employs tile-level encryption with a fixed size of  $16 \times 16$ , achieving finer granularity than Taha's scheme, which uses fixed  $32 \times 32$  tiles and thus inevitably encrypts more non-ROI pixels.

2) *Comparison of ROI Region Perturbation Effect*: The comparison of ROI region perturbation effect includes two parts: comparison of subjective vision and comparison of objective indicators.

**Comparison of Subjective Vision.** Fig. 7 shows the frame #1 and #50 of the Johnny sequence encrypted by five encryption strategies under  $QP = 24$ . Meanwhile, In order to present the distortion difference more clearly, we further slice the ROI region and make a detailed comparison of the distortion effect in Fig. 8. It can be clearly seen from Fig. 8 that the visual distortion of Fig. 8(f) and Fig. 8(l) are the most serious, especially the texture details and contours of the face are almost unrecognizable. This is because the advanced level encryption uses edge scrambling in addition to the encryption syntax elements, causing greater distortion. However, since Yu [16] and Taha [17] both encrypt the IPM, their encryption performance is better than that of the basic level encryption but worse than our enhanced level encryption. The reason is that enhanced level encryption introduces the encryption of

Delta QP and MVPIdx on the basis of basic level encryption which can produce stronger visual distortion.

**Comparison of Objective Indicators.** According to TABLE III, the objective indicators analysis includes: PSNR, SSIM, EDR, information entropy, NPCR, UACI and Bit rate change.

a) *Analysis of PSNR and SSIM*: The testing results of PSNR and SSIM are recorded in TABLE V and TABLE VI, where the optimal results are marked in bold and the suboptimal results are underlined. The results in the following tables of the other indicators are also highlighted in the same way. As can be seen from the tables, the PSNR and SSIM results of the advanced level encryption are almost the optimal and that of the enhanced level encryption are suboptimal. They are both better than that of Yu [16] and Taha [17].

TABLE V AVERAGE PSNR OF THE COMPARED STRATEGIES UNDER DIFFERENT QP

Sequence	QP	Original	Yu [16]	Taha [17]	Basic	Enhanced	Advanced
CLASS_A	8	51.47	<u>11.39</u>	<b>11.30</b>	11.55	11.41	11.69
	24	40.56	11.49	11.60	11.58	<u>11.47</u>	<b>11.20</b>
	40	31.62	11.69	11.82	12.04	<u>11.43</u>	11.49
CLASS_B	8	51.47	13.25	13.16	13.11	<u>13.05</u>	<b>12.86</b>
	24	40.16	<u>13.50</u>	13.60	13.55	13.53	<b>12.49</b>
	40	31.46	13.65	13.51	13.64	<u>13.40</u>	<b>12.85</b>
CLASS_C	8	51.67	13.14	<u>13.11</u>	13.22	13.14	12.21
	24	44.97	13.42	<u>13.34</u>	13.43	13.35	<b>12.01</b>
	40	38.10	12.97	13.12	13.09	<u>12.86</u>	<b>11.86</b>
CLASS_D	8	51.38	13.43	13.32	13.48	<u>13.19</u>	<b>12.72</b>
	24	42.42	13.58	<u>13.50</u>	13.53	13.63	<b>13.26</b>
	40	36.60	13.76	<u>13.61</u>	13.67	13.65	<b>13.54</b>
CLASS_E	8	51.38	12.44	12.55	<u>12.38</u>	12.47	<b>12.10</b>
	24	41.93	12.76	12.66	<u>12.58</u>	12.64	<b>12.12</b>
	40	37.51	12.95	13.06	<u>12.82</u>	12.83	<b>11.94</b>

TABLE VI AVERAGE SSIM OF THE COMPARED STRATEGIES UNDER DIFFERENT QP

Sequence	QP	Original	Yu [16]	Taha [17]	Basic	Enhanced	Advanced
CLASS_A	8	0.997	0.160	0.161	0.173	<u>0.137</u>	<b>0.131</b>
	24	0.972	0.195	0.194	0.206	<u>0.178</u>	<b>0.155</b>
	40	0.903	0.217	0.218	0.245	<b>0.206</b>	0.213
CLASS_B	8	0.998	0.180	0.178	0.189	<u>0.161</u>	<b>0.145</b>
	24	0.996	0.220	0.221	0.230	<u>0.204</u>	<b>0.185</b>
	40	0.820	0.256	0.253	0.263	<u>0.239</u>	<b>0.217</b>
CLASS_C	8	0.995	0.389	0.392	0.410	<u>0.364</u>	<b>0.323</b>
	24	0.971	0.476	0.473	0.503	<u>0.458</u>	<b>0.410</b>
	40	0.919	0.496	0.501	0.504	<u>0.475</u>	<b>0.402</b>
CLASS_D	8	0.996	0.435	0.431	0.428	<u>0.409</u>	<b>0.369</b>
	24	0.943	0.472	0.477	0.457	<u>0.433</u>	<b>0.384</b>
	40	0.876	0.510	0.497	0.510	<u>0.486</u>	<b>0.442</b>
CLASS_E	8	0.997	0.250	0.252	0.263	<u>0.231</u>	<b>0.204</b>
	24	0.969	0.314	0.312	0.327	<u>0.289</u>	<b>0.259</b>
	40	0.856	0.325	0.327	0.338	<u>0.306</u>	<b>0.274</b>

b) *Analysis of Edge Detection*: we first give the encrypted visual effect in edge region of all the compared strategies in Fig. 9. It can be found that Yu [16] and Taha [17] have large edge distortion than the basic level encryption resulting from the perturbation of IPM. However, both the edge distortion of enhanced and advanced level encryption are better than Yu [16] and Taha [17]. The reason is that the enhanced level encryption encrypts MVPIdx and Delta QP and advanced level encryption scramble the edge coefficients, so the advanced level encryption reaches the best results. Meanwhile, the average values of EDR are also listed in TABLE VII. From the table, the advanced level encryption and the enhanced level encryption achieve the optimal and suboptimal results, which are better than Yu [16] and Taha [17]. The result is consistent with the edge image in Fig 9.

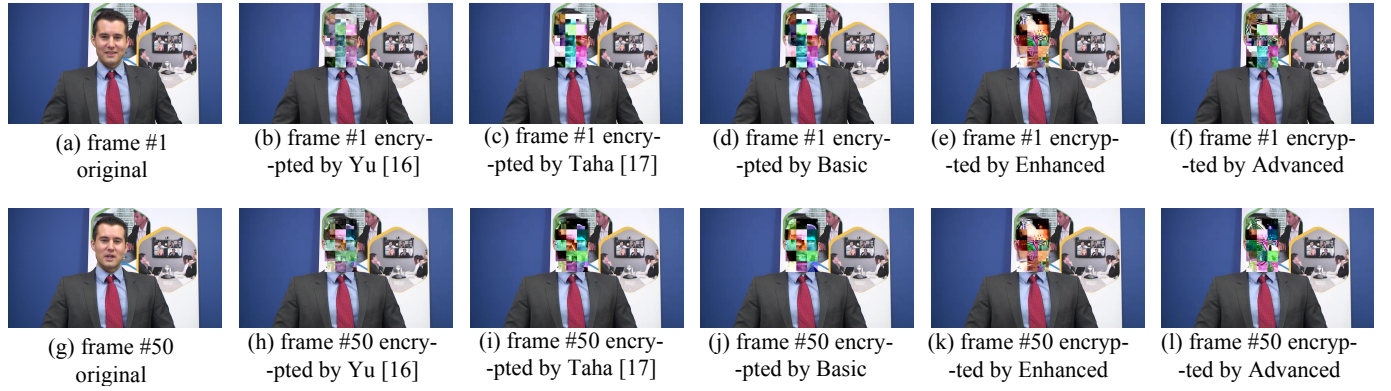


Fig. 7: Subjective vision comparison of the whole frames in Johnny sequence

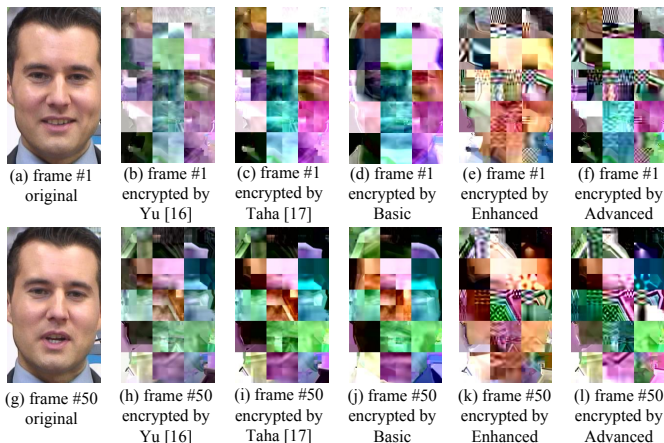


Fig. 8: Subjective vision comparison of the ROI region in Johnny sequence

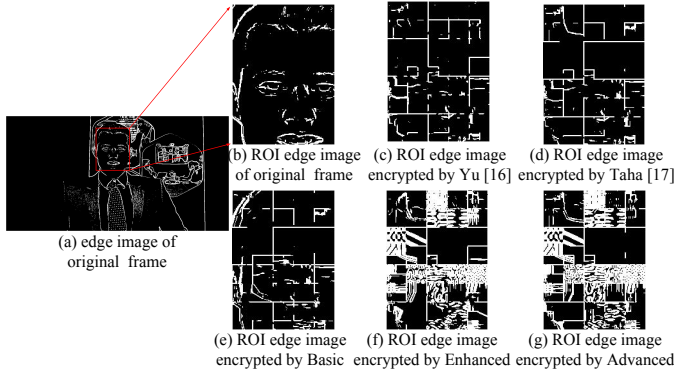


Fig. 9: Edge image comparison of the ROI region in frame #1 in Johnny sequence

TABLE VII AVERAGE EDR OF THE COMPARED STRATEGIES

Sequence	EDR					
	Original	Yu [16]	Taha [17]	Basic	Enhanced	Advanced
CLASS_A	0.11	0.871	0.874	0.824	<b>0.919</b>	<b>0.926</b>
CLASS_B	0.132	0.849	0.849	0.789	<b>0.901</b>	<b>0.908</b>
CLASS_C	0.163	0.841	0.841	0.789	<b>0.902</b>	<b>0.901</b>
CLASS_D	0.307	0.905	0.907	0.831	<b>0.944</b>	<b>0.947</b>
CLASS_E	0.188	0.881	0.882	0.808	<b>0.922</b>	<b>0.923</b>

*c) Analysis of Information Entropy:* the results of the average information entropy of different video sequences in all the compared strategies are shown in Fig. 10. It can be seen that the information entropy of the original video is relatively low, ranging from 6.8 to 7.4, and the information entropy of Yu [16] and Taha [17] is higher. However, the advanced level encryption achieve the highest information entropy, and the result of CLASS\_E reached about 7.95, close to the theoretical maximum value of 8.

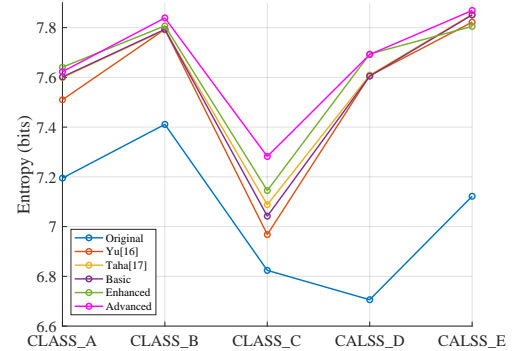


Fig. 10: The comparison of information entropy

*d) Analysis of NPCR and UACI:* The testing results of NPCR and UACI of all the compared strategies are listed in TABLE VIII. the theoretical values of NPCR and UACI are 99.609% and 33.464%, respectively. Therefore. It can be seen from the table that advanced level encryption obtain the optimal NPCR and UACI, which proves it has good resistance to differential attacks.

*e) Analysis of Bit Rate Change:* The experimental results of bit rate change are shown in TABLE IX. From the analysis in Section III-B, whether the encryption of the syntax element will cause an increase in bit rate depends on its entropy coding mode. Encrypting the syntax elements coded by regular mode will inevitably cause an increase in bit rate, Since Yu [16], Taha [17], the enhanced and advanced level encryption all encrypting the syntax elements coded by regular mode, lead to bit rate increment. However, the basic level encryption only encrypts the syntax elements coded by bypass mode, which getting the best results with a zero bit rate increment.

TABLE VIII AVERAGE NPCR AND UACI OF THE COMPARED STRATEGIES

Sequence	NPCR (%)						UACI (%)					
	original	Yu [16]	Taha [17]	Basic	Enhanced	Advanced	original	Yu [16]	Taha [17]	Basic	Enhanced	Advanced
CLASS_A	71.23	<b>99.58</b>	99.56	99.56	99.57	<b>99.57</b>	1.26	<b>29.17</b>	29.00	28.99	29.03	28.16
CLASS_B	71.42	99.40	99.35	99.35	<b>99.41</b>	<b>99.48</b>	1.12	23.97	24.08	24.03	<b>24.64</b>	<b>25.17</b>
CLASS_C	71.73	99.45	99.47	<b>99.48</b>	99.47	<b>99.49</b>	1.29	24.01	<b>24.54</b>	24.53	24.13	<b>24.79</b>
CLASS_D	66.21	<b>99.50</b>	99.46	99.47	99.49	<b>99.66</b>	0.63	<b>27.67</b>	27.33	27.11	27.28	<b>30.53</b>
CLASS_E	69.72	99.49	99.56	<b>99.57</b>	99.53	<b>99.55</b>	0.80	26.13	<b>27.60</b>	<b>27.35</b>	26.67	26.55

TABLE IX AVERAGE BIT RATE CHANGE OF THE COMPARED STRATEGIES

Sequence	Bit Rate Change (%)				
	Yu [16]	Taha [17]	Basic	Enhanced	Advanced
CLASS_A	1.56	1.56	0	2.53	8.11
CLASS_B	1.95	2.02	0	2.77	7.94
CLASS_C	2.23	2.30	0	3.47	10.61
CLASS_D	0.79	0.80	0	2.41	8.8
CLASS_E	1.58	1.60	0	2.71	9.83

## VII. CONCLUSIONS

This paper proposes a tunable scheme and evaluation benchmark for H.265/HEVC ROI encryption, aiming to provide a flexible and efficient privacy protection solution for video applications. By integrating a visual perception network for accurate ROI recognition and a three-level tunable encryption strategy, the scheme is developed to flexibly adapt to varying security and resource requirements. Experimental results demonstrate the scheme's effectiveness in privacy protection while maintaining real-time performance. Additionally, we present a unified ROI encryption evaluation benchmark, providing a standardized quantitative platform for video ROI encryption research. Future research will focus on optimizing the compression efficiency of encryption algorithms, incorporating more advanced object detection technologies, and further improve our evaluation benchmark.

## REFERENCES

- [1] M. Khosravy, K. Nakamura, Y. Hirose, N. Nitta, and N. Babaguchi, "Model inversion attack by integration of deep generative models: Privacy-sensitive face generation from a face recognition system," *IEEE Transactions on Information Forensics and Security*, vol. 17, pp. 357–372, 2022.
- [2] X. Tian, P. Zheng, and J. Huang, "Robust privacy-preserving motion detection and object tracking in encrypted streaming video," *IEEE Transactions on Information Forensics and Security*, vol. 16, pp. 5381–5396, 2021.
- [3] Y. Hirose, K. Nakamura, N. Nitta, and N. Babaguchi, "Anonymization of human gait in video based on silhouette deformation and texture transfer," *IEEE Transactions on Information Forensics and Security*, vol. 17, pp. 3375–3390, 2022.
- [4] D. Kim and C. Guyot, "Optimized privacy-preserving cnn inference with fully homomorphic encryption," *IEEE Transactions on Information Forensics and Security*, vol. 18, pp. 2175–2187, 2023.
- [5] P. Carrillo, H. Kalva, and S. Magliveras, "Compression independent object encryption for ensuring privacy in video surveillance," in *2008 IEEE International Conference on Multimedia and Expo*, pp. 273–276, IEEE, 2008.
- [6] F. Dufaux and T. Ebrahimi, "H. 264/avc video scrambling for privacy protection," in *2008 15th IEEE International Conference on Image Processing*, pp. 1688–1691, IEEE, 2008.
- [7] F. Dufaux and T. Ebrahimi, "Scrambling for privacy protection in video surveillance systems," *IEEE Transactions on Circuits and Systems for Video Technology*, vol. 18, no. 8, pp. 1168–1174, 2008.
- [8] K. M. Hosny, M. A. Zaki, H. M. Hamza, M. M. Fouda, and N. A. Lashin, "Privacy protection in surveillance videos using block scrambling-based encryption and dcnn-based face detection," *IEEE Access*, vol. 10, pp. 106750–106769, 2022.
- [9] R. Li, J. Hou, H. Yu, and X. Li, "Ppl-enc: A personalized pixel-level scheme for video privacy protection," in *2024 IEEE/ACM 32nd International Symposium on Quality of Service (IWQoS)*, pp. 1–10, IEEE, 2024.
- [10] T. Stutz and A. Uhl, "A survey of h. 264 avc/svc encryption," *IEEE Transactions on circuits and systems for video technology*, vol. 22, no. 3, pp. 325–339, 2011.
- [11] J. Xu, J. Guo, and J. Bao, "A roi encryption scheme for h. 264 video based on moving object detection," in *2013 2nd International Symposium on Instrumentation and Measurement, Sensor Network and Automation (IMSNA)*, pp. 494–497, IEEE, 2013.
- [12] Q. Sheng, C. Fu, Z. Lin, J. Chen, X. Wang, and C.-W. Sham, "Content-aware tunable selective encryption for hevc using sine-modular chaoticification model," *IEEE Transactions on Multimedia*, 2024.
- [13] G. Van Wallendael, A. Boho, J. De Cock, A. Munteanu, and R. Van de Walle, "Encryption for high efficiency video coding with video adaptation capabilities," *IEEE Transactions on Consumer Electronics*, vol. 59, no. 3, pp. 634–642, 2013.
- [14] F. Peng, X.-w. Zhu, and M. Long, "An roi privacy protection scheme for h. 264 video based on fmo and chaos," *IEEE transactions on information forensics and security*, vol. 8, no. 10, pp. 1688–1699, 2013.
- [15] S.-K. Im and K.-H. Chan, "Cabac-based roi encryption with mask r-cnn for vvc codec," in *2024 18th International Conference on Ubiquitous Information Management and Communication (IMCOM)*, pp. 1–6, IEEE, 2024.
- [16] J.-Y. Yu and Y.-G. Kim, "Coding unit-based region of interest encryption in hevc/h. 265 video," *IEEE Access*, vol. 11, pp. 47967–47978, 2023.
- [17] M. A. Taha, N. Sidaty, W. Hamidouche, O. Dforges, J. Vanne, and M. Viitanen, "End-to-end real-time roi-based encryption in hevc videos," in *2018 26th European Signal Processing Conference (EUSIPCO)*, pp. 171–175, IEEE, 2018.
- [18] H. Sohn, E. T. AnzaKu, W. De Neve, Y. M. Ro, and K. N. Plataniotis, "Privacy protection in video surveillance systems using scalable video coding," in *2009 Sixth IEEE international conference on advanced video and signal based surveillance*, pp. 424–429, IEEE, 2009.
- [19] M. Farajallah, W. Hamidouche, O. Déforges, and S. El Assad, "Roi encryption for the hevc coded video contents," in *2015 IEEE International Conference on Image Processing (ICIP)*, pp. 3096–3100, IEEE, 2015.
- [20] A. Bochkovskiy, C.-Y. Wang, and H.-Y. M. Liao, "Yolov4: Optimal speed and accuracy of object detection," *arXiv preprint arXiv:2004.10934*, 2020.
- [21] P. Viola and M. Jones, "Rapid object detection using a boosted cascade of simple features," in *Proceedings of the 2001 IEEE computer society conference on computer vision and pattern recognition. CVPR 2001*, vol. 1, pp. I–I, Ieee, 2001.
- [22] L. Jiao, F. Zhang, F. Liu, S. Yang, L. Li, Z. Feng, and R. Qu, "A survey of deep learning-based object detection," *IEEE access*, vol. 7, pp. 128837–128868, 2019.
- [23] K. He, G. Gkioxari, P. Dollár, and R. Girshick, "Mask r-cnn," in *Proceedings of the IEEE international conference on computer vision*, pp. 2961–2969, 2017.
- [24] X. Wang, R. Zhang, T. Kong, L. Li, and C. Shen, "Solov2: Dynamic and fast instance segmentation," *Advances in Neural information processing systems*, vol. 33, pp. 17721–17732, 2020.
- [25] J. Redmon and A. Farhadi, "Yolov3: An incremental improvement," *arXiv preprint arXiv:1804.02767*, 2018.
- [26] A. Krizhevsky, I. Sutskever, and G. E. Hinton, "Imagenet classification with deep convolutional neural networks," *Advances in neural information processing systems*, vol. 25, 2012.

- [27] S. Ren, K. He, R. Girshick, and J. Sun, "Faster r-cnn: Towards real-time object detection with region proposal networks," *Advances in neural information processing systems*, vol. 28, 2015.
- [28] D. Flynn, D. Marpe, M. Naccari, T. Nguyen, C. Rosewarne, K. Sharman, J. Sole, and J. Xu, "Overview of the range extensions for the hevc standard: Tools, profiles, and performance," *IEEE Transactions on Circuits and Systems for Video Technology*, vol. 26, no. 1, pp. 4–19, 2015.
- [29] D. Marpe, H. Schwarz, and T. Wiegand, "Entropy coding in video compression using probability interval partitioning," in *28th Picture Coding Symposium*, pp. 66–69, IEEE, 2010.
- [30] F. Liu and H. Koenig, "A survey of video encryption algorithms," *computers & security*, vol. 29, no. 1, pp. 3–15, 2010.
- [31] B. Tang, C. Yang, and Y. Zhang, "A format compliant framework for hevc selective encryption after encoding," *IEEE Transactions on Circuits and Systems for Video Technology*, vol. 33, no. 3, pp. 1140–1156, 2022.
- [32] H. Lipmaa, P. Rogaway, and D. Wagner, "Ctr-mode encryption," in *First NIST Workshop on Modes of Operation*, vol. 39, Citeseer. MD, 2000.
- [33] Y. Zhang, D. Xiao, W. Wen, and Y. Tian, "Edge-based lightweight image encryption using chaos-based reversible hidden transform and multiple-order discrete fractional cosine transform," *Optics & Laser Technology*, vol. 54, pp. 1–6, 2013.
- [34] F. Peng, X. Zhang, Z.-X. Lin, and M. Long, "A tunable selective encryption scheme for h. 265/hevc based on chroma ipm and coefficient scrambling," *IEEE Transactions on Circuits and Systems for Video Technology*, vol. 30, no. 8, pp. 2765–2780, 2019.
- [35] J. Wang, X. Li, J. Chen, L. Zhou, L. Guo, Z. He, H. Zhou, and Z. Zhang, "Dph-yolov8: Improved yolov8 based on double prediction heads for the uav image object detection," *IEEE Transactions on Geoscience and Remote Sensing*, 2024.